Joint Centre for Mesoscale Meteorology, Reading, UK

Contributions of the JCMM/ Dept of Meteorology Radar Group to the 27th AMS Radar Meteorology Conference, Vail October 1995

Internal Report No. 50

June 1995

Met Office Joint Centre for Mesoscale Meteorology Department of Meteorology
University of Reading PO Box 243 Reading RG6 6BB United Kingdom
Tel: +44 (0)118 931 8425 Fax: +44 (0)118 931 8791
www.metoffice.com

Designed and produced by the Met Office © Crown copyright 2001 01/0240 The Met Office logo is a registered trademark.

CONTRIBUTIONS OF THE JCMM/DEPT OF METEOROLOGY RADAR GROUP

TO THE 27TH AMS RADAR METEOROLOGY CONFERENCE, VAIL OCTOBER 1995

1. Density and size distribution of aggregating snow particles inferred from coincident aircraft and radar observations.

by

J W G Thomason, A J Illingworth and V Marecal

Aggregating ice particles have spectra: $N(D)=No\ exp(-\Lambda D)$, with No proportional to Λ^3 obeyed over a wide range of No. Best agreement with the 3GHz radar is obtained if the ice particles have density 0.92 g/cm³ for D<0.5mm, and ≈0.1g/cm³ for D>0.5mm.

2. Sizing of ice aggregates and snowflakes using coincident 3 and 35GHz reflectivity observations.

by

A J Illingworth, J W G Thomason, J W F Goddard, H Sauvageot and P Simpson.

Snowflakes undergo Mie scattering at 35GHz and Rayleigh at 3GHz. The mean size is derived from the ratio of the reflectivities.

3 Dual wavelength polarisation measurements in precipitation using the CAMRA and Rabelais radars.

by

J W F Goddard, K L Morgan, A J Illingworth and H Sauvageot

In heavy rain the 35GHz signal is attenuated by 30dB: a value predicted by simultaneous 3GHz observations of Z and Z_{DR}, thus confirming the validity of drop shapes and scattering theory.

4 Simultaneous differential phase measurements at 3 and 35GHz.

by

T M Blackman, A J Illingworth, J W F Goddard and H Sauvageot

These are the first measurements at 35GHz. The size of melting particles can be estimated by comparing the differential phase shift on backscatter to the differential reflectivity.

5. Differential Doppler Velocity (DDV) - a third parameter for characterising particle size distributions.

by

D R Wilson, A J Illingworth and T M Blackman

Simultaneous Doppler and polarisation radar observations at 3GHz depend on both the terminal velocity and the shape of raindrops, so the third parameter 'm' of a gamma distribution can be found.

6. The effect of ice crystal density on the radar reflectivity of clouds at millimetric wavelengths.

by

M E J Gosset, A J Illingworth, P R A Brown and J W G Thomason

Computations of 94GHz radar reflectivity, based on ice spectra from aircraft, show that the reduced ice density of the larger cirrus particles has a large effect; this lower density may also be important for retrievals based on lidars and radiometers.

P2.21 DENSITY AND SIZE DISTRIBUTION OF AGGREGATING SNOW PARTICLES INFERRED FROM COINCIDENT AIRCRAFT AND RADAR OBSERVATIONS

John W. G. Thomason*, Anthony J. Illingworth and Virginie Marécal

JCMM, University of Reading
Reading, UK

1. INTRODUCTION

The interpretation of radar reflectivity for aggregating snow is normally problematic because of the unknown concentrations, sizes and densities of the ice particles. A combination of radar and coincident aircraft microphysical data, however, provides a powerful tool for the investigation of aggregate size spectra, densities and growth processes.

Aggregates tend to have size spectra of the form,

$$N = N_0 \exp(-\lambda D) \qquad (1)$$

where D is the particle diameter (mm), and N the concentration (m^{-4}). The parameters N_0 and λ are used in the cloud microphysical schemes of mesoscale models, and are currently calculated as N_0 = constant and λ = f(IWC), as in, for example, Rutledge and Hobbs (1983), but it may be possible to refine these schemes with a more thorough understanding of the processes involved.

The present research uses high resolution reflectivity data from the Chilbolton 3GHz radar in Southern England, which has a beamwidth of only 0.25° and a range resolution of 300 m, in conjunction with *in situ* PMS optical probe measurements from the UK Meteorological Research Flight C-130 aircraft. The 2DP and 2DC optical probes provide two-dimensional particle images with resolutions of 200 μm and 25 μm respectively, from which diameters and shapes can be retrieved using a suitable image analysis program. The shape information is used to verify that the particles involved are predominantly aggregates.

Three flights in stratiform precipitation (maximum Z ≈ 30 dBZ) were studied (A016-June 21 1990, A296-November 9 1993 and A354-October 19 1994), each consisting of a series of level runs of approximately 70 km at a variety of heights corresponding to temperatures between 0 and -15°C.

*Corresponding author address: John W. G. Thomason, Department of Meteorology, University of Reading, Reading RG6 2AU, UK.

2. OPTICAL PROBE SPECTRA

With the particle diameters obtained from the optical probe data it is possible to reconstruct size spectra for the aircraft runs. These runs are split into 10 s (≈ 1 km) segments, which provide samples of several thousand particles, which is a suitable number to produce the spectra, whilst maintaining sufficient resolution to observe spatial variability on approximately the same scale as seen by the radar. A typical spectrum, consisting of merged 2DP/2DC data is shown in figure 1. The spectrum can be divided into two distinct regimes. Above ≈ 500 μm it can be characterised by an exponential distribution as in (1) with intercept, N_0 (m^{-4}), and gradient, λ (mm^{-1}), determined by a best fit line through the data. Below 500 μm there is also an approximately exponential spectrum, but with intercept N_{0C} and gradient λ_C. This behaviour is observed in virtually all of the flights.

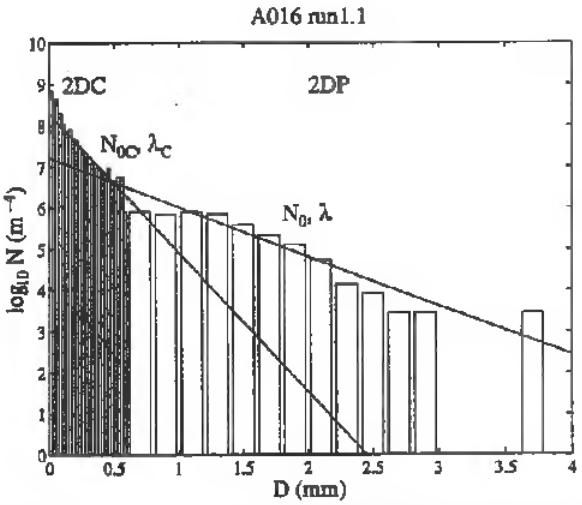

Figure 1 A typical 10 s merged 2DP/2DC spectrum from the optical probe images.

The values of N_0 and λ obtained for the particles larger than 500 μm are highly correlated, as can be seen in figure 2, which includes the values for each of the three flights studied. For the individual flights the relationships vary between $N_0 = 5.43\times10^5\lambda^{2.90}$ (A016) and $N_0 = 3.17\times10^5\lambda^{3.48}$ (A296). These are in excellent agreement with the theoretical calculations of Passarelli (1978), which predict an equilibrium relationship for aggregate particles in steady stratiform precipitation given by,

$$N_0 = C\lambda^3 \qquad (2)$$

where C depends on the updraught speed, lapse rate and snowfall type. If a straight line is fitted through the data from each flight such that in each case the exponential in the N_0-λ relationship is constrained to be exactly 3.0, in accordance with Passarelli's theory, then appropriate values of C can be found. These vary between 5.09×10^5 (A016) and 4.97×10^5 $m^{-4}mm^3$ (A296). The values are remarkably consistent with one another, considering the diversity of conditions for the individual flights.

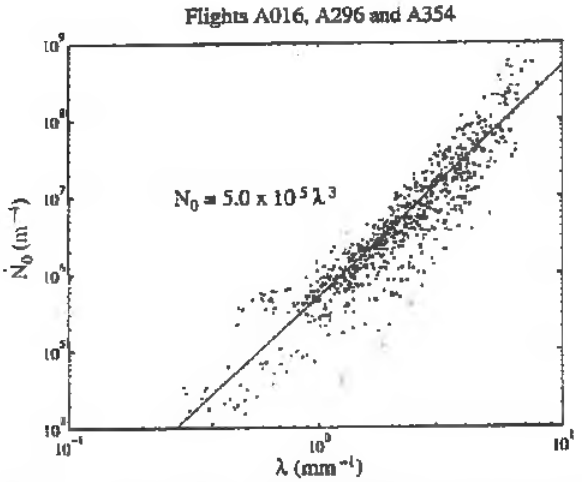

Figure 2 N_0, λ values from the 2DP spectra for all the flights.

It is interesting to note that when Houze *et al.* (1979) performed a similar comparison with Passarelli's theory no positive evidence for (2) was found. This may have been a consequence of taking N_0 and λ from spectra averaged over entire runs, rather than from shorter segments, causing the dynamic range of the data to collapse into a much smaller area, and making any correlation harder to distinguish.

None of the data recorded is inconsistent with the relationship $N_0 = 5\times10^5\lambda^3$, which is shown as a solid line in figure 2, and is obeyed even though the values of N_0 extend over five orders of magnitude. This may prove extremely useful in the parameterization of snow and ice aggregation processes in mesoscale models.

3. REFLECTIVITY AND IWC RETRIEVAL

For comparison with the actual radar reflectivity (Z) which, at 3GHz, is assumed to be governed by the Rayleigh approximation, information on the expected reflectivity (Z_{2D}) can be determined from the particle images using,

$$Z_{2D} = \frac{1}{V}\sum_{i=1}^{n}\frac{|K|^2(\rho_i)}{0.93}D_i^6 \quad [mm^6m^{-3}] \qquad (3)$$

where the summation is carried out over the n particles in the volume V (m^3), D_i (mm) is the particle diameter and $|K|^2$ a factor dependent upon its complex refractive index and hence its density (ρ_i). The value of Z_{2D} is normalized to that for a single 1 mm rain drop (which has $|K|^2 = 0.93$) in the same volume V.

The particle density (ρ) could be assigned using a standard relationship for aggregates such as $\rho = 0.07D^{-1.1}$ from Locatelli and Hobbs (1974), but this predicts vanishingly small values of ρ and hence K^2 for large D, whereas there is no clear physical reason why aggregates, themselves growing by aggregation, should decrease in density with size.

The simplest approach is to assume a constant aggregate ρ for all values of D, and optimize this by minimizing the differences between Z_{2D} and Z. This, however, ignores the cloud microphysics which demands that the smallest particles, growing via the diffusion of water vapour, should actually be solid crystals.

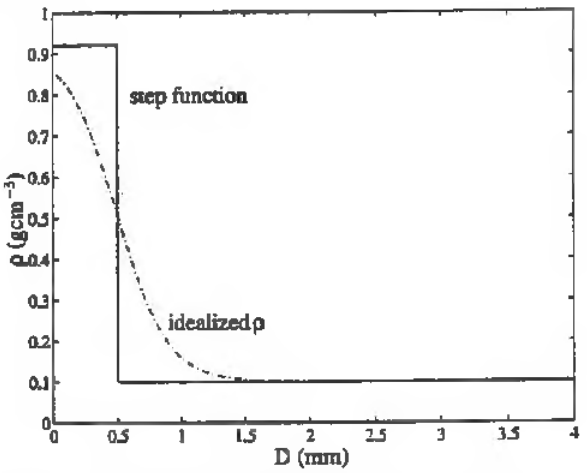

Figure 3 Idealized (dot-dashed) and step (solid) density functions.

Figure 1 suggests the possibility that there are, in fact, two populations of particles, defined by the distributions characterised by N_0, λ (aggregates, $\rho \approx 0.1$ gcm^{-3}) and N_{0C}, λ_C (solid ice, $\rho = 0.92$ gcm^{-3}). If this is assumed then an idealized ρ can be calculated from the contributions of the two distributions across the range of D, as shown in figure 3. To simplify calculations this idealized ρ is replaced by a ρ function with a step at 500 μm and an aggregate ρ which can again be determined by optimization.
Figure 4 shows the Z_{2D} results produced with the constant ρ and step function schemes for one run of flight A354. Clearly the step function is much more effective in reproducing Z, particularly for low values of Z, where the reflectivity is biased towards smaller D. The fact that this is also the case in every other run provides evidence that the assumptions made in invoking a ρ step function are valid.

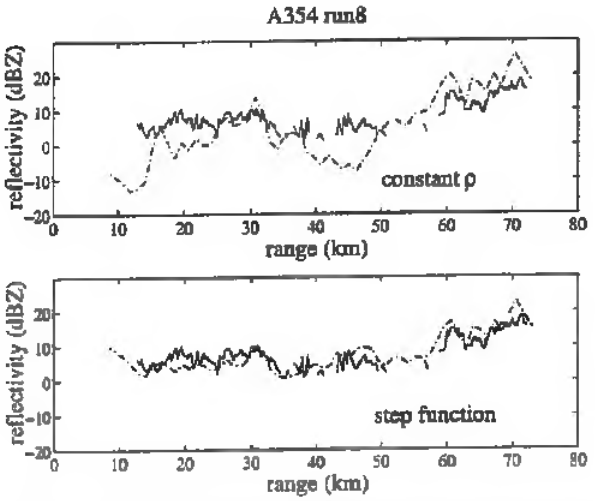

Figure 4 Z (solid) and Z_{2D} (dot-dashed) for constant and step function densities.

When comparing Z_{2D} with Z it is important to realise that spatial and temporal variations in the cloud structure can be relatively large. Thus a single radar image, recorded over a few seconds, may not be representative of a run lasting more than ten minutes. The most reliable method is to construct a composite radar image from a number of others, preferably with (as on this day) each having evidence of a hit on the aircraft, indicating alignment to within ≈ 200 m. It is imperative that the radar and aircraft measurements should be coincident if quantitative information is to be derived from the comparison, and this has undoubtedly been a difficulty in other studies such as Marécal *et al.* (1993).

Values of aggregate ρ in stratiform precipitation are found to be between 0.07 and 0.1 gcm^{-3}, except at temperatures above -5°C, where they can rise to 0.25 gcm^{-3}, presumably as a result of riming.

Once these values of ρ have been determined they can be used to derive other parameters such as IWC. This can be calculated using,

$$IWC_{2D} = \frac{1}{V}\frac{\pi}{6000}\sum_{i=1}^{n} \rho_i D_i^3 \quad [gm^{-3}] \qquad (4)$$

and hence a general relationship for IWC = f(Z) can be determined. This is found to be,

$$IWC = 0.034Z^{0.40} \qquad (5)$$

with IWC in gm^{-3} and Z in mm^{6}m^{-3}, which compares well with IWC = $0.037Z^{0.50}$ (Heymsfield (1977)). This relationship works well even though Z can vary by two orders of magnitude and temperature by 15°C.

4. ACKNOWLEDGMENTS

We should like to thank RAL for the use of the Chilbolton radar and MRF for supplying optical probe data. This research was funded by grants from NERC (GR3/8765 and GST/02/718), ESTEC (7815/93) and CEC (EV5V-CT94-0463).

5. REFERENCES

Heymsfield, A. J., 1977: Precipitation development in stratiform ice clouds: a microphysical and dynamical study. *J. Atmos. Sci.*, **34**, 367-381

Houze Jr., R. A., P. V. Hobbs, D. B. Parsons and P. H. Herzegh, 1979: Comments on "Size distributions of precipitation particles in frontal clouds", reply. *J. Atmos. Sci.*, **37**, 699-700

Locatelli, J. D. and P. V. Hobbs, 1974: Fall speeds and masses of solid precipitation particles. *J. Geophys. Res.*, **79**, 2185-2197

Marécal, V., D. Hauser and C. Duroure, 1993: Airborne microphysical measurements and radar reflectivity observations near a cold frontal rainband observed during the FRONTS 87 experiment. *Atmos. Res.*, **29**, 179-207

Passarelli Jr., R. E., 1978: An approximate analytical model of the vapour deposition and aggregation growth of snowflakes. *J. Atmos. Sci.*, **35**, 118-124

Rutledge, S. A. and P. V. Hobbs, 1983: The mesoscale and microscale structure and organization of clouds and precipitation in midlatitude cyclones. VIII: a model for the "seeder-feeder" process in warm-frontal rainbands. *J. Atmos. Sci.*, **40**, 1185-1206

3.6 SIZING OF ICE AGGREGATES AND SNOWFLAKES USING COINCIDENT 3 AND 35 GHZ REFLECTIVITY OBSERVATIONS

Anthony J. Illingworth*, John W. G. Thomason, John W. F. Goddard†, Henri Sauvageot‡ and Patrick M. Simpson

JCMM, University of Reading, Reading, UK

†Rutherford Appleton Laboratory, UK

‡University Paul Sabatier, France

1. INTRODUCTION

Radar reflectivity measurements at 35GHz and 3GHz have been used to estimate the size spectra of aggregating snowflakes. As the size of the snowflakes increases so the Mie scattering progressively reduces the 35GHz reflectivity, Z_{35}, relative to the 3GHz value, Z_3. The value of the dual wavelength ratio, Z_3/Z_{35}, or DWR, rises above unity, with its magnitude being a measure of the mean size of the snowflakes. Once the size is known then the concentration can be found from Z_3 which is unaffected by Mie scattering. The size spectra derived from the radar are consistent with those from coincident *in situ* aircraft data.

The use of DWR to infer hydrometeor size was first proposed for hail detection by Atlas and Ludlam (1961) at 9GHz and 3GHz, but corrections must be made for attenuation at 9GHz (e.g. Tuttle and Rinehart, 1983). In practice it is almost impossible to disentangle the reduction in Z at 9GHz due to Mie scattering by the hailstones, from the attenuation at 9GHz caused by the heavy rain or by the hailstones which could be either wet or dry. Such ambiguities are much reduced for snowflakes, which, because of their low density and dryness, undergo Mie scattering at 35GHz without any accompanying attenuation.

Accurate measurements of DWR are only possible if the beamwidths are well matched with a common sample volume, otherwise even quite modest reflectivity gradients which are always present, will swamp the DWR signal (Gosset and Sauvageot, 1993). Matrosov (1992) demonstrated that over a whole PPI the average value of Z_{35} is reduced below that of Z_3, but because the beams were not aligned he could not retrieve detailed spectra. The 3GHz data presented here are taken with the 0.25° beamwidth, 25m RAL Chilbolton antenna and the 35GHz data with a smaller 0.4°,1.4m antenna rigidly attached to the outer rim of the 25m dish so that the two scan together. Observations of the sun confirm that the two radars are coaxially aligned to better than 0.1°.

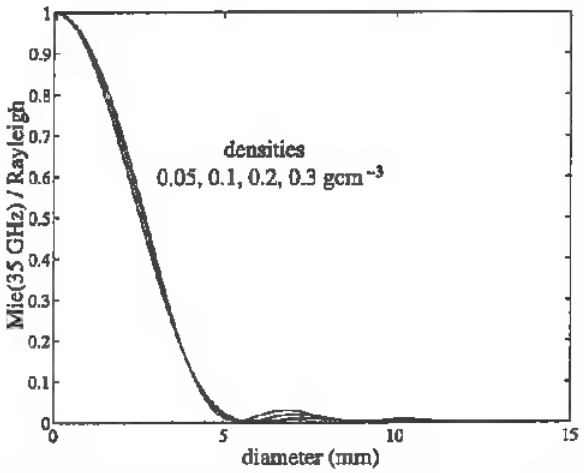

Figure 1 The ratio of Mie to Rayleigh backscatter for ice spheres at 35GHz.

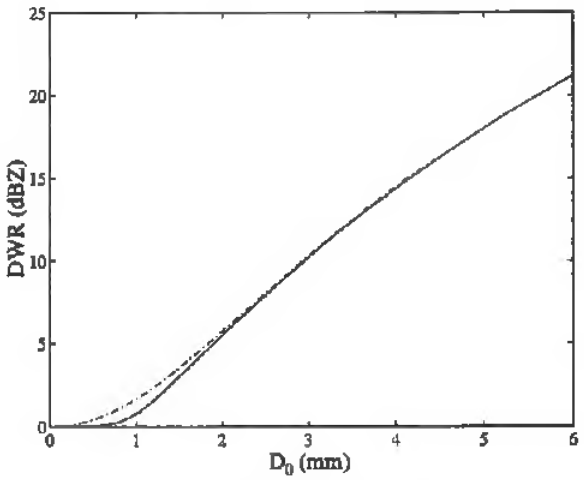

Figure 2 DWR for constant (dot-dashed) and step (solid) density functions.

*Corresponding author address: Anthony J. Illingworth, Department of Meteorology, University of Reading, Reading RG6 2AU, UK.

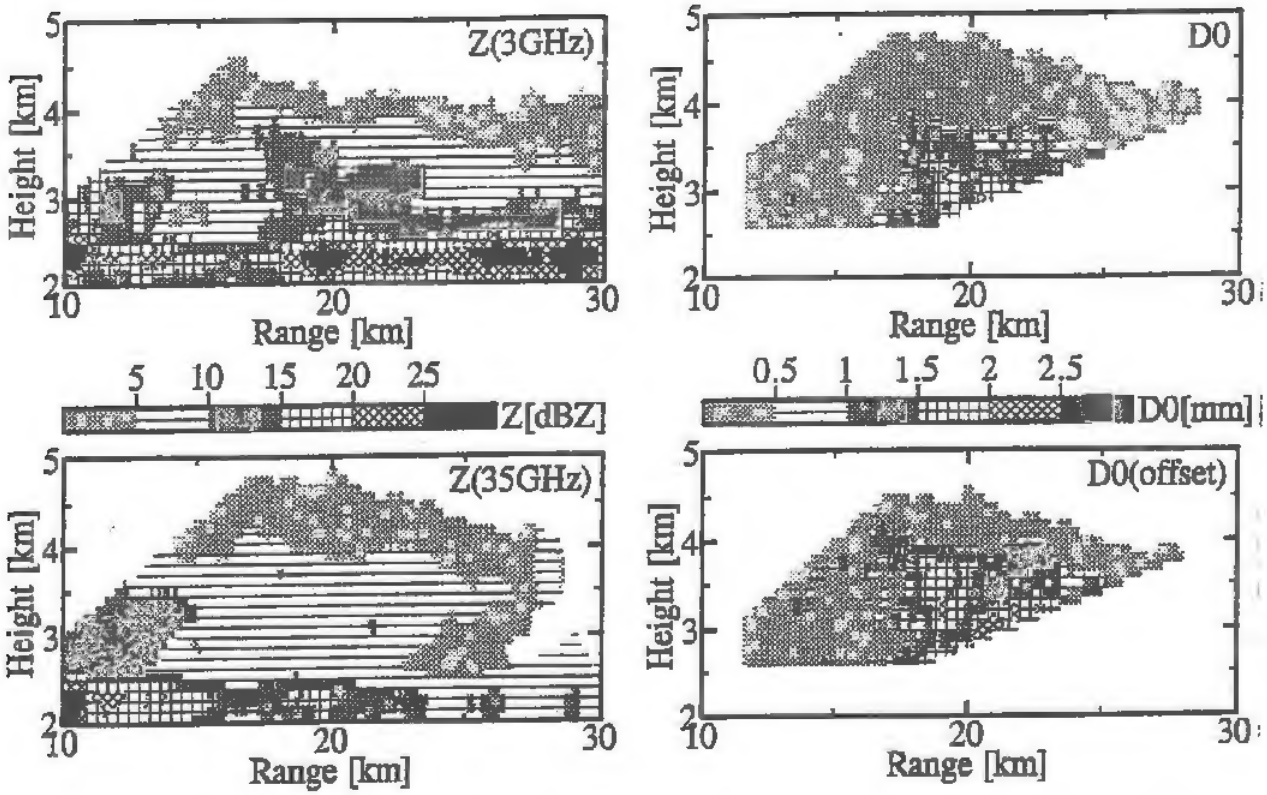

Figure 3 Vertical section of reflectivities and D_0 through stratiform snow, 19 October 94 at 1020 GMT.

2. DUAL WAVELENGTH THEORY

The theoretical ratio of Mie to Rayleigh backscatter for ice spheres at 35GHz as a function of their diameter is plotted in figure 1 for various densities showing that it falls to 50% for 3mm spheres but is only weakly dependent upon density. If we consider a distribution of ice particles of the form,

$$N(D) = N_0 \exp(-3.67\ D/D_0) \qquad (1)$$

then the theoretical values of DWR as a function of D_0 are displayed in figure 2 for two models of ice particle density. One curve is for a constant ice density of $0.1 gcm^{-3}$, the second uses a density step function with solid ice below 0.5mm and a constant value of $0.1 gcm^{-3}$ for larger sizes. The value of N_0 is found from,

$$Z_3 = N_0 \int \frac{|K|^2}{0.93} \exp(-3.67\ D/D_0)\ D^6\ dD \qquad (2)$$

where the 0.93 arises because Z_3 is expressed relative to water drops. For a constant density of $0.1 gcm^{-3}$ this reduces to,

$$N_0 = 4.85\times10^6\ Z_3/D_0^7 \qquad (3)$$

where N_0 is in m^{-4} and D_0 in mm. A comparison of radar reflectivities and aircraft data (Thomason *et al.*, 1995) suggests that the step function in density is more realistic and hence we shall use this for the retrieval of values of N_0 in this paper. Low density snowflakes reflect as if they are spheres, thus justifying our model assumption that the particles could be considered spherical.

3. DUAL FREQUENCY OBSERVATIONS

The RHI of Z_3 and Z_{35} in figure 3 shows the bright band at 2.4km with stratiform precipitation above. Before attempting retrievals of D_0 we must consider the uncertainty in DWR, which could be due to noise in the Z estimates, relative calibration errors, and attenuation at 35GHz from rain and water vapour.

The noise in the Z_3 signal, which is determined by the 250msec dwell and spatial averaging over four 75m gates, is equal to 0.7dB, the noise in the Z_{35} signal being much less. The attenuation in rain is large at 35GHz, so the technique adopted was to match Z_{35} to Z_3 as the radar beam left the cloud; D_0 values were only retrieved when Z_3 at cloud top fell below 5dBZ, where, according to our calculations, there should be no Mie scattering at 35GHz. Only

those values of D_0 which satisfy these criteria are plotted in figure 3. For water vapour at 35GHz, Sauvageot (1982) quotes a two way attenuation of 0.02dB/km per gm^{-3}. Assuming saturated vapour at 800mb and -10°C, the predicted attenuation over the final 10km of the radar path is only 0.5dB, which is small enough to be neglected.

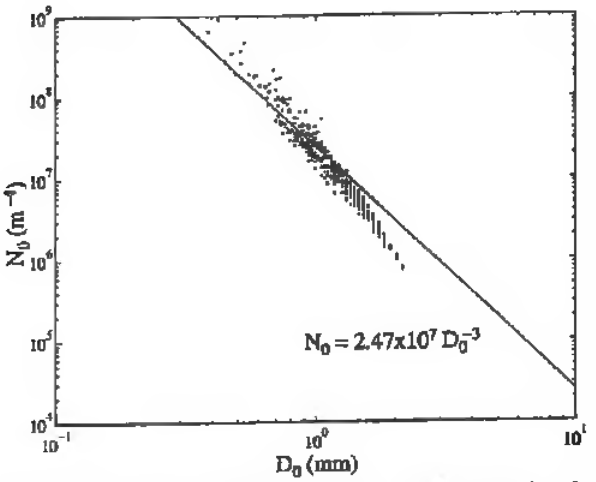

Figure 4 N_0, D_0 retrieval from the vertical section in figure 3.

In order to quantify the errors introduced by a system with non-aligned radar beams, two retrieved fields of D_0 are displayed in figure 3. The upper plot uses the observed data, but in the lower plot, 'D_0 offset', one Z field has been shifted vertically by 300m to simulate a 1° beam misalignment. The large difference in the two fields of D_0 confirms that even a small offset leads to unacceptable errors. Figure 4 shows the corresponding values of N_0 and D_0, together with the relationship $N_0 = 2.47 \times 10^7 D_0^{-3}$ obtained from aircraft runs through this cloud in the 30 minutes before and after the RHI. The figure confirms that the radar retrievals for stratiform snowfall are consistent with *in situ* data from the aircraft, although we need more data in stratiform snowfall for D_0 above 2mm, that is Z_3 above 15dBZ. Retrievals on other days through more broken echoes from small cells of higher reflectivity and convective elements reveal a very different pattern of N_0 and D_0 from the simple one in stratiform snowfall displayed in figure 4.

We now consider the sensitivity in the errors of the retrieved values of D_0 and N_0 for a DWR error of 0.7dB. The errors in D_0 can be found from figure 2 which predicts that if D_0 is 1mm then a 0.7dB error in DWR leads to a retrieval error of about 0.3mm (30% or 1dB); if D_0 is 4mm, then the error falls to 0.2mm (5% or 0.2dB). The N_0 errors are much higher. If N_0 is approximately proportional to Z_3/D_0^7, then this leads to an error in N_0 of 8dB for D_0 = 1mm, and 2dB for a D_0 of 4mm. Further work is needed to quantify these errors more closely and to refine the corrections for attenuation, but we still conclude that the retrievals in figure 4 are consistent with the aircraft observations.

4. CONCLUSIONS

These observations demonstrate that ice particle sizes can be inferred from dual wavelength observations provided the radar beams are very precisely matched. The technique relies on the low density of snowflakes so that Mie scattering at 35GHz is not accompanied by attenuation. We are presently installing a 94GHz radar to derive cirrus ice particle sizes in the range 0.5 to 1.5mm.

5. ACKNOWLEDGMENTS

We thank RAL for the use of the Chilbolton radar and the Meteorological Research Flight for the aircraft data. This research was funded by grants from NERC (GR/H 49054 and GR/3 8765), ESTEC (7815/93) and CEC (EV5V-CT94-0463).

6. REFERENCES

Atlas, D. and F. H. Ludlam, 1961: Multi-wavelength radar reflectivity of hailstorms. *Q. J. Roy. Meteorol. Soc.*, 87, 524-534

Gosset, M. and H. Sauvageot, 1992: A dual wavelength radar method for ice-water characterisation. *J. Atmos. and Oceanic Technol.*, 9, 538-547

Matrosov, S. Y., 1992: Radar reflectivity in snowfall. *IEE Trans. Feo. and Rem. Sensing*, 30, 454-461

Sauvageot, H., 1992: Radar Meteorology. Artech House, 366pp

Thomason, J. W. G., A. J. Illingworth and V. Marécal, 1995: Density and size distribution of aggregating snow particles inferred from coincident aircraft and radar observations. *These proceedings.*

Tuttle, J. D. and R. E. Rinehart, 1983: Attenuation correction in dual-wavelength analyses. *J. Clim. and Appl. Meteorol.*, 22, 1914- 1921

5B.8 DUAL-WAVELENGTH POLARISATION MEASUREMENTS IN PRECIPITATION USING THE CAMRA AND RABELAIS RADARS

John W F Goddard *, Kevin L. Morgan
Rutherford Appleton Laboratory, UK

Anthony J. Illingworth
JCMM, Dept. of Meteorology, University of Reading, UK

Henri Sauvageot
University Paul Sabatier, France

1. INTRODUCTION

Polarisation radars are increasingly being utilised in application areas as diverse as hydrology and communications systems studies, both because of their ability to characterise raindrop size distributions, and their ability to distinguish ice and water phases. The Chilbolton CAMRa radar has been used over a number of years in conjunction with satellite beacons at X, Ku and Ka band, where slant path attenuation, differential attenuation and differential phase have been inferred from S-band data. This paper describes how similar techniques have been adopted to estimate attenuation and differential attenuation, due to rain, for comparison with values obtained directly from the 35 GHz Rabelais radar, which is co-located on the 25m Chilbolton antenna.

2. THE CAMRA AND RABELAIS RADARS

The CAMRa radar is an S-band system, capable of simultaneous measurement of horizontally polarised reflectivity, Z_H, differential reflectivity, Z_{DR}, cross-polar reflectivity, LDR, differential phase, Φ_{DP}, and Doppler velocity, Goddard et al. (1994). The radar beamwidth is 0.25°, and the range gate length is normally 300m. The 35 GHz Rabelais radar, on loan from the University Paul Sabatier, France, is mounted on the side of the 25m antenna, and it's own 1.4m dish provides a 0.4° beamwidth, precisely aligned with the 3 GHz beam.

This configuration allows direct ray-by-ray comparison of both reflectivity and differential reflectivity between the two frequencies. The assumption is then made that S-band attenuation due to both rain and atmospheric gases is negligible for the relatively modest events analysed here, so that differences between S-band and Ka-band reflectivity or differential reflectivity can be ascribed to a combination of non-Rayleigh scattering and rain attenuation at the higher frequency.

Both these effects can also be estimated from the S-band measurements, under certain assumptions regarding drop shape and drop size distribution, and the magnitude of the estimates compared with that inferred from the S-band and Ka-band differences. The next section describes these relationships.

A third effect, gaseous absorption, is by no means negligible at Ka-band. Two way absorption values of 0.16 dB km^{-1} for water vapour, assuming a water vapour density of 7.5 g m^{-3}, and 0.06 dB km^{-1} for molecular oxygen, have been applied here, ITU-R (1992).

3. RELATIONSHIPS BETWEEN S-BAND AND Ka-BAND PARAMETERS

Polarisation radar measurements of reflectivity and differential reflectivity enable the two parameters, D_0, the median volume diameter, and N_0, in the gamma DSD:

$$N(D) = N_0 D^{\mu} \exp\left(-\left(\frac{3.67+\mu}{D_0}\right)D\right) \qquad (1)$$

to be determined for each radar range gate, assuming a specific value for μ. In the analysis that follows, an exponential DSD has been assumed, with $\mu = 0$.

With the DSD characterised in this way, the specific attenuation for a horizontally polarised wave at 35 GHz, A_{H35}, and the differential specific attenuation, A_{HV35}, normalised by the reflectivity at 3 GHz, can both be computed as a function of

* *Corresponding author address:*
John W F Goddard, RCRU,
RAL, Chilton, Didcot, Oxon OX11 0QX, UK
e-mail: j.goddard@rl.ac.uk

differential reflectivity at 3 GHz. The results, for a one-way path, shown in Figures 1(a) and 1(b) were computed using the Fredholm Integral Method (FIM) described by Holt et al (1978). It should be noted that the differential attenuation curve is very sensitive to the relation between the effective rain drop oblateness and diameter. The form of this relation, based on extensive comparisons between radar and distrometer data, (for example of these, see Bringi et al (1984)), is:

$$\begin{aligned} q/b &= 1.075 - 0.065D - 0.0036D^2 + 0.0004D^3 \quad \text{for } D > 1.1mm \\ q/b &= 1 \qquad\qquad\qquad\qquad\qquad\qquad\quad \text{for } D \le 1.1mm \end{aligned} \tag{2}$$

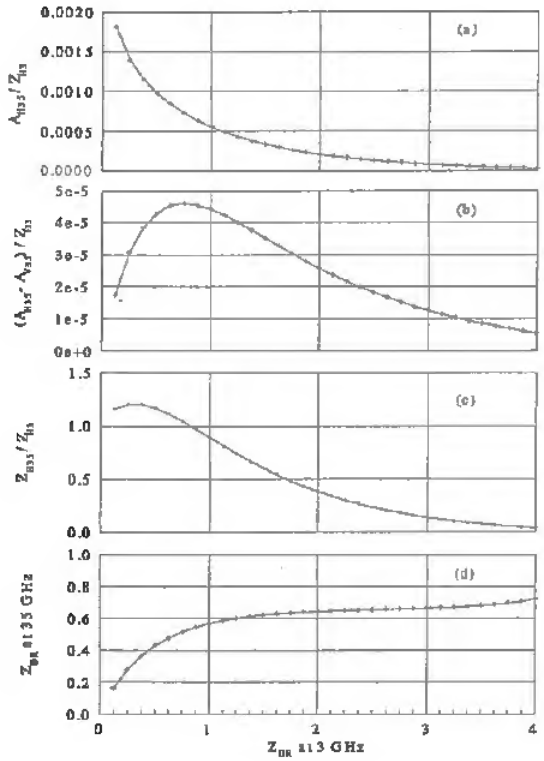

Figure 1: Normalised Ka-band (one-way) attenuation (a), differential attenuation (b) and reflectivity (c), and Ka-band differential reflectivity (d), as a function of S-band differential reflectivity.

Figure 1(c) gives the normalised Ka-band reflectivity, while figure 1(d) gives values of Z_{DR} at Ka-band computed from drop size distributions that result in the given values of Z_{DR} at S-band. Non-Rayleigh scatter at the higher frequency drastically reduces Z_{DR}, compared with S-band values, and, as expected, the effect is independent of N_0, and hence, reflectivity, depending solely on D_0, and, hence, Z_{DR}.

4. VERIFICATION OF ATTENUATION AND MIE SCATTER CORRECTION ALGORITHMS

Coincident S and Ka-band reflectivity measurements along a ray at an elevation of 1.4° are shown in figure 2, with the corresponding differential reflectivity measurements in figure 3. It is clear from figure 2 that the effect of attenuation at Ka-band caused by moderate rain over less than 10 km is quite dramatic: of the order of 30 dB on the two-way path.

We can now use the results of figure 1(a) to compute Ka-band attenuation, A_{H35}, on a gate-by-gate basis, from each S-band measurement of Z_H and Z_{DR}, and use the results to correct the measured Ka-band reflectivity. This gives the curve labelled 'Ka-band corrected for attenuation' in fig. 2. To confirm the validity of the attenuation estimates, we first have to calculate the true Ka-band reflectivity, allowing for Mie effects. These can be predicted from the measured S-band Z_H and Z_{DR} values through curve (c) in fig. 1.

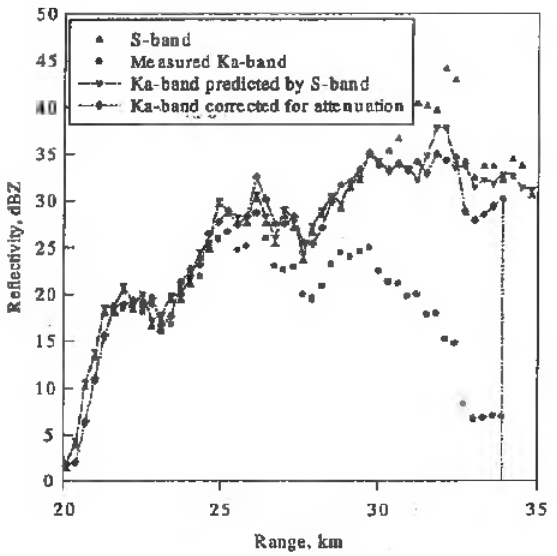

Figure 2: S-band and Ka-band reflectivity measurements on 24 October 1994 at 2249 GMT

As expected, the Mie scatter effects are negligible in the weak rain, but in the stronger rain, where S-band Z_{DR} values of up to 3 dB occur (see fig. 3, below), Ka-band reflectivities are reduced by up to 5 dB. Such differences are, of course, much more pronounced in the melting layer, where the very large effective diameters of particles cause the virtual disappearance of the 'bright band' so common at

lower frequencies (see, for example, Russchenberg and Ligthart, (1993)).

Excellent agreement between the attenuation-corrected Ka-band reflectivities and the Mie-corrected reflectivities is obtained, as shown in fig. 2. In like manner, we can use the information from figure 1 to analyse the differential reflectivity signatures that correspond to the reflectivity values in figure 2. These measurements are shown in figure 3, where we have already noted that the S-band Z_{DR} values approach 3 dB in the most intense precipitation, whereas the Ka-band values simply become increasingly negative due to the combined effects of differential attenuation and non-Rayleigh scatter.

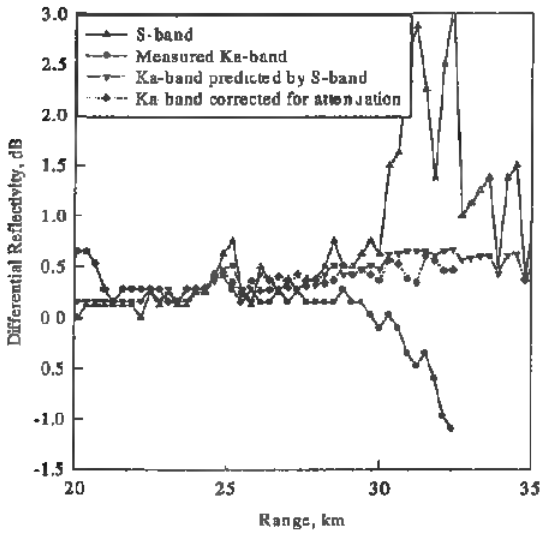

Figure 3: S-band and Ka-band differential reflectivity measurements on 24 October 1994 at 2249 GMT.

The relative magnitude of these two factors can be discerned by comparing the Ka-band Z_{DR} values predicted from the S-band Z_{DR} measurements, using figure 1(d). The effect of Mie scatter is to limit the maximum Ka-band Z_{DR} values to about 0.6 dB. Differential attenuation then further reduces the measured Ka-band differential reflectivity, by nearly 2 dB. Also shown in figure 3 is the correction for the Ka-band differential attenuation, deduced from the S-band measurements through figure 1(b). These yield values in excellent agreement with the expected Ka-band values that allow for Mie scatter.

5. CONCLUSIONS

The principal conclusion to be drawn from these comparisons is that the scattering theory and the underlying assumptions concerning drop shape and size distribution provide a reliable framework within which to interpret radar data. For specific applications, such as the use of radar data to model both the attenuating and scattering effects of rain on communications systems, these results provide considerable justification for further development.

Future work will extend this analysis to quantify the attenuation and scattering properties of the melting layer, and compare with models that have been developed for this purpose.

6. ACKNOWLEDGEMENTS

The research activity reported in this paper has been performed as part of the National Radio Propagation Programme at RAL, and has been funded by the Radiocommunications Agency of DTI. NERC Grant No. GR/H49054 supported the installation at Chilbolton of the Ka-band radar. Our thanks are also due to Dr Jun Tan, who computed the scattering parameters used in figure 1.

7. REFERENCES

Bringi, V.N., J.W.F. Goddard and S. M. Cherry, 1982: Comparison of dual-polarisation radar measurements of rain with ground-based disdrometer measurements, *J. Appl. Met.*, **21**, 252-264.

Goddard, J.W.F., J.D. Eastment and M. Thurai, 1994: The Chilbolton Advanced Meteorological Radar: a tool for multidisciplinary atmospheric research. *Electronics & Communication Engineering J.*, April, 77-86.

Holt, A.R., , N.K. Uzunoglu and B.G. Evans, 1978: An Integral Equation Solution to the Scattering of Electromagnetic Radiation by Dielectric Spheroids and Ellipsoids, *IEEE-Trans. Ant. and Prop., AP26*, 5, 706-712.

ITU-R, 1992: Attenuation by Atmospheric Gases in the Frequency Range 1 350 GHz, RPN Series Propagation in Non-Ionised Media, Rec. 676-1.

Russchenberg, H. W. J. and L.P.Ligthart, 1993: A Doppler-polarimetric backscatter model of the melting layer, *IEE Conf. Publ. 370-2*, 877-880.

9A.9

SIMULTANEOUS DIFFERENTIAL PHASE MEASUREMENTS AT 3 AND 35 GHZ.

T Mark Blackman*, Anthony J Illingworth*, John W F Goddard† and Henri Sauvageot‡

*JCMM, University of Reading, Reading, UK

†Rutherford Appleton Laboratory, UK

‡Universite Paul Sabatier, Toulouse, France

1. INTRODUCTION

Observations of the phase difference (ϕ_{DP}) between Z_H and Z_V, the reflectivities measured with horizontal and vertical polarisation, have been made at 3 and 5.6GHz (e.g. Bringi et al, 1991). Previous studies have used the gradient of ϕ_{DP} with range (called K_{DP}, the specific propagation differential phase) to estimate rainfall rate (Sachidananda and Zrnic, 1986). K_{DP} is a propagation effect; as the rain becomes heavier and the drops more oblate, the speed of the horizontally polarised wave falls below that of the vertical wave.

In this paper we report the first measurements of ϕ_{DP} at 35GHz (λ = 8.6mm). They are taken with the co-located 3 and 35GHz radars at Chilbolton (Goddard et al, 1995). At 35GHz particles larger than a few mm undergo Mie scattering and there can be significant differential phase shift on backscatter (δ), which, in light precipitation, can dominate the propagation effects. Large values of δ occur in the melting layer, and our observations suggest that a combination of differential reflectivity, Z_{DR}, and δ, can provide rather precise estimates of the mean size and shape of the particles in the bright band.

TABLE 1

Z_{DR} (dB) and δ at 35GHz for wet oblates.
(Raindrop shapes in **bold**)

AXIAL RATIO				SIZE(mm)
0.75	0.85	0.9	0.95	
3.1/3°	1.8/2°	1.1/1°	0.6/1°	1
3.4/8°	1.9/4°	1.3/3°	0.6/1°	1.5
3.1/14°	1.8/8°	1.2/5°	**0.6/3°**	2
2.2/18°	1.2/11°	**0.8/7°**	0.4/3°	2.5
1.1/19°	**0.6/11°**	0.4/7°	0.2/3°	3
-3.0/0.7°	-1.2/5°	-0.7/4°	-0.3/2°	4

*Corresponding author address: T Mark Blackman, Department of Meteorology, University of Reading, Reading RG6 2AU, UK.

2. DIFFERENTIAL PHASE SHIFT AT 35GHZ

Theoretical values of both Z_{DR} and δ at 35GHz for wet oblates with various axial ratios as a function of size are given in table 1. The Z_{DR} of raindrops peaks at only +0.8dB for 2 to 3mm size before Mie scattering causes it to go negative above 4mm. The predicted values of K_{DP} in rain (figure 1) at 35GHz behave similarly. For light rain Rayleigh scattering is applicable, K_{DP} scales with frequency and is about ten times higher than the 3GHz value, but for raindrop diameters > 4mm , Mie scattering reduces K_{DP} so that it is negative for rain > 30 or 60mm/hr. K_{DP} is sensitive both to the index 'm' of an assumed gamma raindrop size distribution (Ulbrich, 1982) and to the drop shape model (Blackman and Illingworth, 1995); here the drop shapes of Goddard et al (1995) are used.

Table 1 predicts that, for melting ice particles which have some degree of alignment in the horizontal and are < 3mm, the combination of Z_{DR} and δ should provide an accurate estimate of a mean size and shape. Equivalent dry ice particles have a lower dielectric constant so Z_{DR} and δ are much reduced.

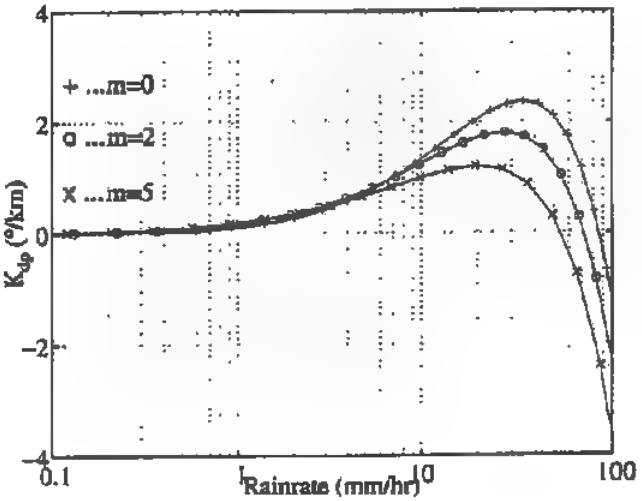

Figure 1 Theoretical K_{DP} in rain at 35GHz.

27th AMS Conference on Radar Meteorology
Vail, Colorado, USA
October, 1995

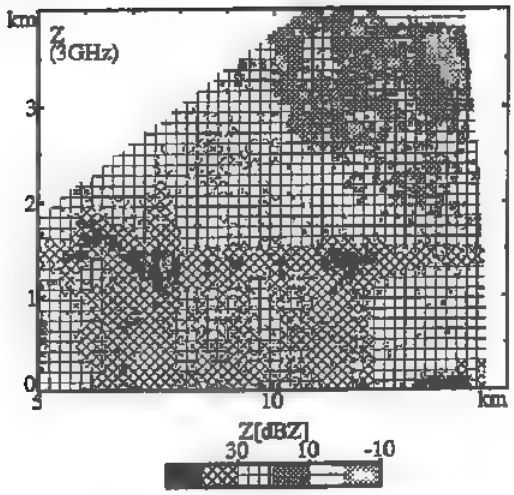

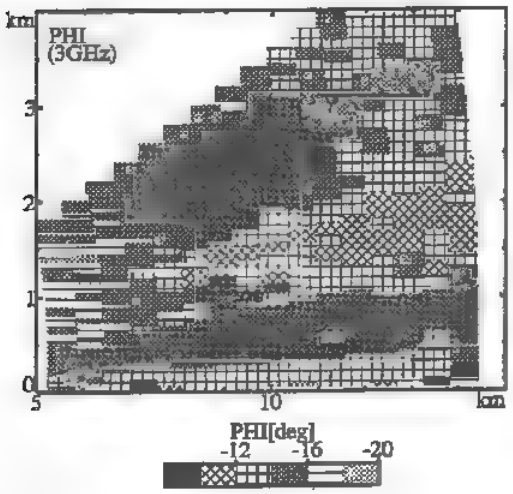

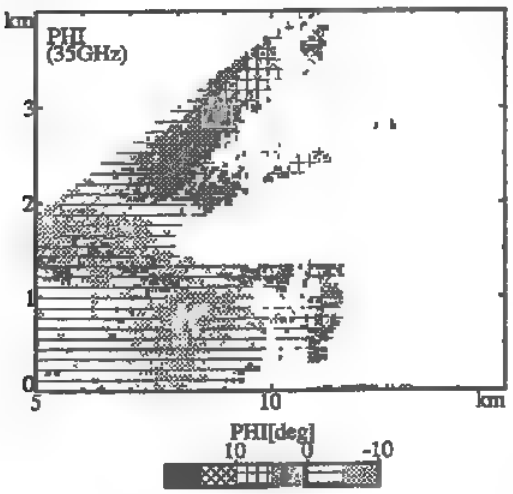

Figure 2. RHI through heavy precipitation

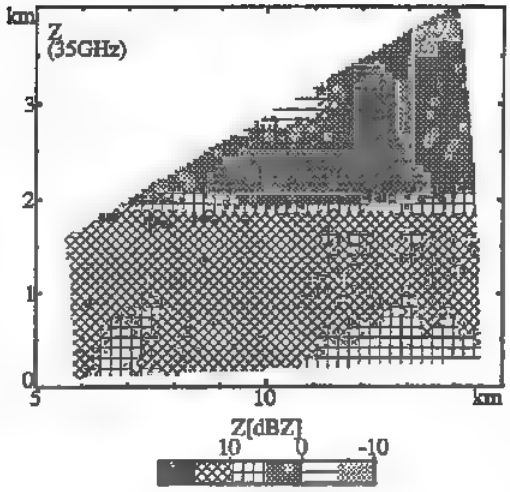

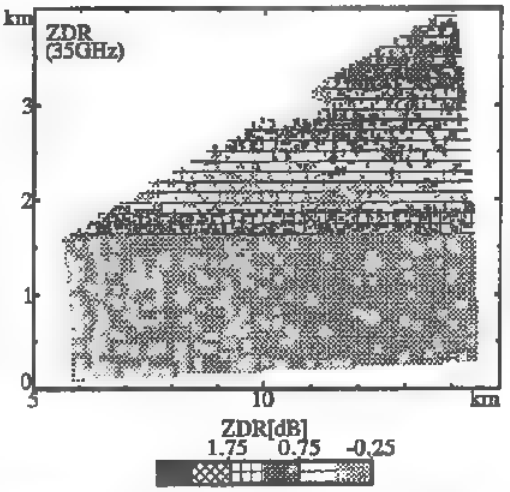

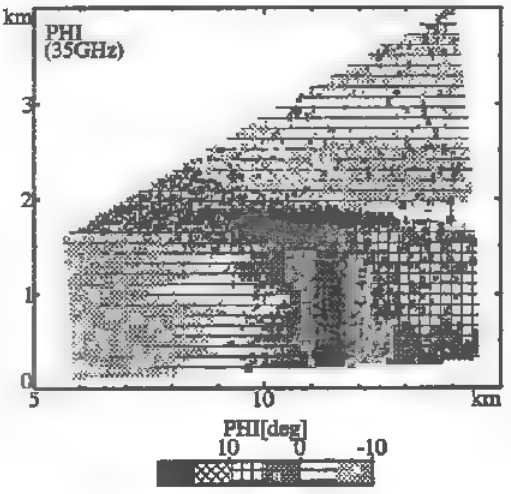

Figure 3. RHI through light precipitation

3. OBSERVATIONS

Values of Z at 3GHz and ϕ_{DP} at both 3 and 35GHz for an RHI in heavy rain are displayed in figure 2. Z exceeds 40dBZ in the bright band (height 1.3km) and is over 30dBZ in the rain below. 3GHz phase shifts over the 10km path in the rain total about 1°, and in the ice 2°; in the bright band the low correlation makes ϕ_{DP} values at 3GHz noisy (not discernable in the figure) but there is an obvious jump in ϕ_{DP} of about 5° across the more intense parts of the bright band. At 35GHz the shifts along 10km paths in ice are about 20° (ten times higher - indicating that Rayleigh scatter is valid in the ice), but in the rain there is evidence that significant δ is superposed on any K_{DP} trend. At 35GHz the bright band is associated with a peak in ϕ_{DP} of about 10° to 15° which is due to δ. Severe attenuation makes interpretation of Z and Z_{DR} at 35GHz very difficult.

A second case study at 35GHz is shown in figure 3 in much lighter and rather uniform precipitation with Z < 15dBZ. In this case the 35GHz values of Z and Z_{DR} are unaffected by attenuation. A typical ray profile at 10.7° in figure 4 illustrates the features more quantitatively.

Z values increase about 10dB in passing from ice to rain indicating high density ice particles. In this very light rain Z_{DR} is zero, as expected; it peaks at about 1.8dB in the bright band and then falls to 0.5dB in the ice above. In figure 4 the most obvious feature in ϕ_{DP} is the roughly constant value in both the rain and the ice on which a sharp maximum δ of about 10° is superposed, which coincides with the bright band.

The Z and Z_{DR} profiles are consistent with small ice particles melting in the bright band. The values of Z_{DR} and δ in the bright band are about 1.8dB and 10°, indicating (table 1) that the mean size and axial ratio of the particles are close to 2.25mm and 0.85. The equivalent dry ice particle of density 0.92g cm^{-3} would have a Z_{DR} of 1dB and a δ of 1°, but actual values of Z_{DR} in the ice are about 0.5dB (figure 4) suggesting a slightly lower ice density.

Some features in the ice are puzzling; there is a slight minimum in ϕ_{DP} about 500m above the bright band. This feature is often seen in heavier stratiform precipitation at 3GHz. Electrical effects should be negligible and so cannot explain it. We find it difficult to explain the large phase shifts (2°/km) in the light rain where Z_{DR} is almost zero.

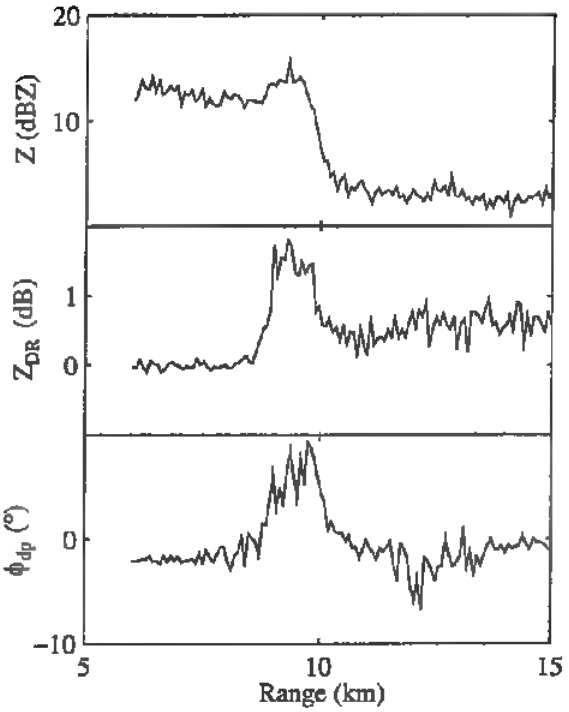

Figure 4. A 35GHz ray profile through figure 3.

4. CONCLUSIONS

We suggest that in light precipitation, if there are wet particles which are more oblate than raindrops, ϕ_{DP} at 35GHz may be dominated by differential phase shift on backscatter, δ. The two observables Z_{DR} and δ may then be used to provide precise measurements of a mean size of ice cloud particles as they melt.

5. ACKNOWLEDGMENTS

This research was funded by grants from NERC (GST/02/0917 and GR3/8765), ESTEC (7815/93) and CEC (EV5V-CT-94-0463).

6. REFERENCES

Blackman T.M and A J Illingworth, 1995, Improved measurements of rainfall using differential phase techniques. Cost-75 Int Seminar, Kluwer.

Goddard,J.W.F.,K.L.Morgan,A.J.Illingworth and H. Sauvageot, 1995. Dual-wavelength polarisation measurements in precipitation using the Camra and Rabelais radars. These proceedings.

Sachidananda, M and Zrnic, D 1986, Differential propagation phase-shift and rainfall rate estimation. Radio Sci, 21, 235-247.

Ulbrich, C.W., 1983, Natural variations in the analytical form of the raindrop-size distribution. J Climate Appl Meteor, 22, 1764-1775.

10A.4 DIFFERENTIAL DOPPLER VELOCITY (DDV) - A THIRD PARAMETER FOR CHARACTERISING PARTICLE SIZE DISTRIBUTIONS.

Damian R. Wilson*, Anthony J. Illingworth, T. Mark Blackman

JCMM, Department of Meteorology,
University of Reading,
Reading, U.K.

1. INTRODUCTION

Two independent radar measurements can, in principle, be fitted to an exponential particle size distribution; an example is the use of Z and Z_{DR} in rain where Z_{DR} is the ratio of Z_H to Z_V, the reflectivities measured using horizontal and vertical polarization, respectively. A three parameter gamma distribution of the form

$$N(D) = N_0 D^m \exp\left(-\frac{(m+3.67)}{D_0} D\right), \qquad (1)$$

provides a more realistic representation with the index, 'm', providing a measure of the breadth of the distribution; positive values of m leading to a more monodispersed spectrum and introducing a natural truncation. Direct measurement of m from distrometers is difficult due to the large number of drops which must be sampled to obtain a reliable estimate. Ulbrich and Atlas (1984) calculated Z, Z_{DR}, and rainfall rate from distrometer data and found that m=2 gave consistent results. Goddard and Cherry (1984b) found the best agreement between radar observations of Z and Z_{DR} and ground based distrometer data was for m=5.

We present measurements of a new parameter, the Differential Doppler Velocity or DDV, mainly in rain but also in the melting layer and in the ice, and compare them with theoretical calculations. Such data could help with the understanding of processes which must be parameterized in mesoscale models such as evaporation of rain and aggregation of ice particles.

2 THE MEASUREMENT TECHNIQUE

The measurement technique combines polarization and fall velocity data obtained by observing Doppler velocities, v_H and v_V, at horizontal and vertical polarization at a significant elevation angle, typically twenty degrees, so that there is a significant Doppler component of the fall velocities, but the values of Z_{DR} are only slightly reduced. Metcalf (1986) looked at the Doppler velocity differences between the two orthogonal circularly polarized channels, but in this paper we use linear polarizations, which may be easier to interpret for particles having a degree of horizontal alignment. The two mean velocities, v_H and v_V, calculated using the pulse pair estimator are then subtracted, leaving a residual term, the DDV. In this paper we will always quote the vertical component of DDV obtained by dividing the observed DDV by the sine of the elevation angle. The theoretical spectra of v_H and v_V for rain are plotted in figure 1; in rain the larger drops are more oblate so the mean v_H is greater than the mean v_V and DDV is positive.

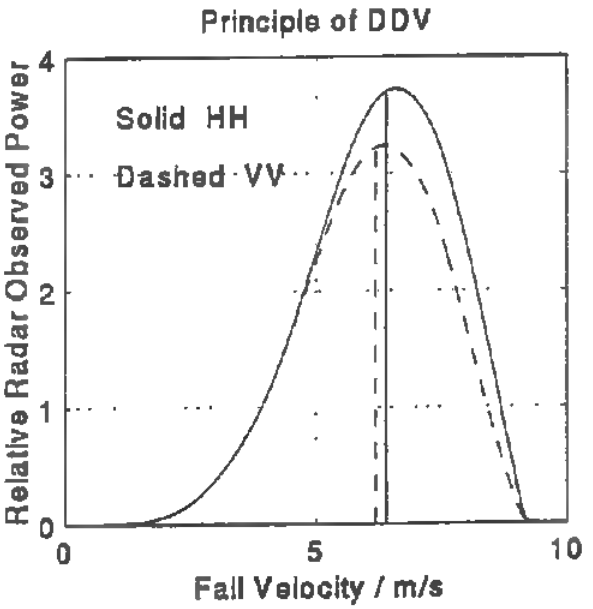

Figure 1. The Doppler velocity spectra in rain.

The magnitude of DDV is much less than the widths of the individual Doppler spectra. Methods which rely on the Doppler width to estimate 'm', for example, Russchenberg (1993), fail because the

*Corresponding author address: Damian R. Wilson, JCMM, Department of Meteorology, University of Reading, Reading, RG6 2AU, U.K.

observed width is dominated by turbulence. The advantage of DDV is that the turbulence affects the horizontally polarized and vertically polarized spectra equally and so DDV is unaffected.

3 RESULTS

The results presented below were recorded by the 10cm RAL Chilbolton radar in Hampshire U.K. which transmits alternate horizontal and vertical polarizations at 610Hz with a range resolution of 75m and a maximum unambiguous velocity of ± 7.6 m/s.

The narrow 0.25 degree beam of the radar means that the beam should be uniformly filled with particles advecting at a constant velocity. In high shear regions, Metcalf (1986) points out that the horizontal velocities of large and small particles can differ; this effect is small in the data discussed in this paper.

3.1 A Typical Dwell in Rain and Ice.

Typical DDV values at each 75m gate for a 10 second dwell in the rain, melting layer and ice are displayed in figure 2; the mean and standard error are derived by splitting the dwell into 8 subsections. As expected, DDV in the rain is positive, with a value of around 0.15m/s. In the ice DDV is very close to zero but slightly negative in places, consistent with more

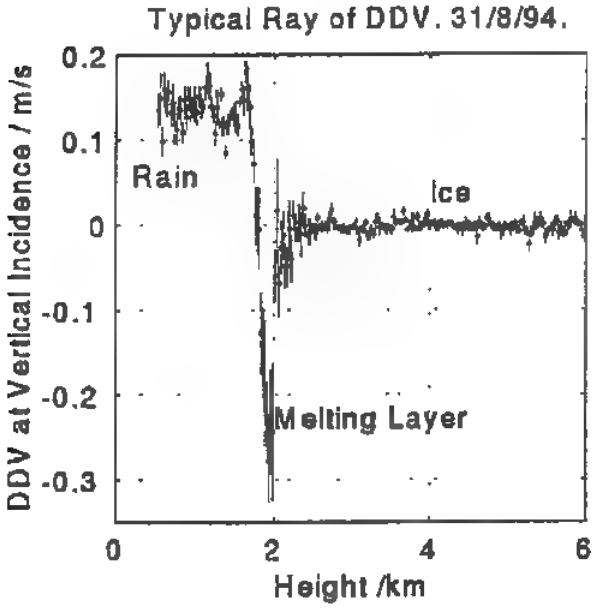

Figure 2. Typical DDV values for a dwell taken at 20 degrees elevation. The mean and standard error in the DDV values are shown.

slowly falling particles such as crystals having larger intrinsic Z_{DR} values. Within the melting layer DDV becomes extremely negative; this is probably due to a mixture of spherical water droplets and slower falling wet snowflakes which are oblate. Typically, DDV in the melting layer is around -0.25m/s although values higher than -0.35m/s have been observed.

3.2 Measurement of m for Rain Spectra.

Z_{DR} and DDV are independent of the overall scaling factor N_0 and the theoretical plots for rain in figure 3 show a significant change in the relationship between DDV and Z_{DR} for different values of m. These curves were calculated using the Beard and Chuang (1987) drop shapes modified by Goddard and Cherry (1984a) and truncated at 8mm, together with the Gunn and Kinzer (1949) fall velocities.

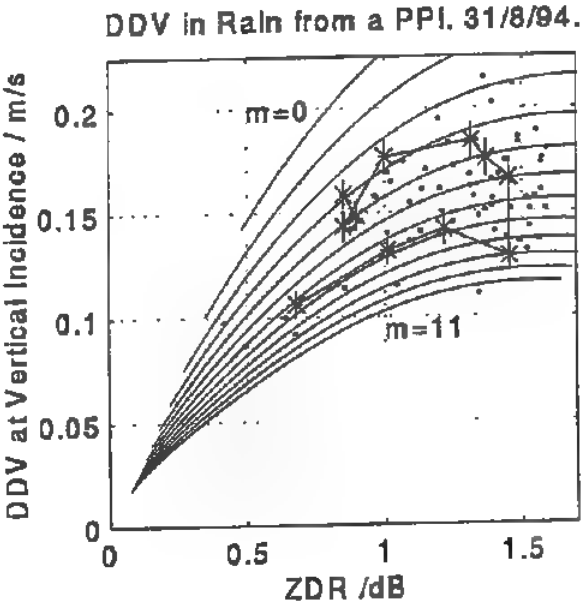

Figure 3. Theoretical and observed values of Z_{DR} and DDV in rain.

Plotting measurements on this grid ought to reveal the value of m in each case. The data points superposed on figure 3 are for a PPI in rain at 10 degrees elevation with a scan rate of 1 degree per second. Because of the inherent noise in the estimator due to the Doppler width, sizeable averaging had to be performed, in this case over 2000 pulse pairs (7 degrees) and 8 range gates, which is equivalent to a spatial scale of about 1km. The data points joined by lines in figure 3 correspond to a 7km path in rain

along one particular ray; the error bars are derived empirically from the variance of the DDV and Z_{DR} estimates from the individual time series. For clarity, error bars have been omitted for other data points in the PPI, which are displayed as dots. Figure 3 demonstrates that there is a real variation in m with values between about 2 to 8 being detected. Measurements from other scans suggest that m=5 is a reasonable average over a large range of rainfall rates although there is always a spread of values. No DDV values above the m=0 line have been observed. Once m and D_0 have been derived from figure 3 the value of N_0 can be calculated from the observed Z value.

3.3 Measurement of DDV in Ice.

DDV is always much lower in magnitude in ice than it is in the rain. Typical values of DDV range from 0 m/s to -0.05 m/s, although values below -0.1 m/s have been recorded. DDV is well correlated with Z_{DR}, suggesting that two particle types are probably present, which could be spherical aggregates and high Z_{DR} crystals having a smaller fall velocity. As the proportion of aligned crystals decreases, Z_{DR} falls, and the spread in terminal velocities is less, leading to a decrease in DDV. Typically DDV shows a decrease of around 0.05 m/s for every 1dB increase in Z_{DR}, although there is large spread in the observations; in some regions there is no DDV but substantial Z_{DR} suggesting the presence of a single crystal type only.

4 CONCLUSIONS

DDV is a new radar parameter which can be implemented on dual-polarization Doppler radars. It combines polarization and fall velocity data in such a way that is independent of turbulence and moderate shears in the atmosphere. DDV responds to ranges of particle size where shape and terminal velocity are changing rapidly. For rain, this weights DDV to drops both slightly smaller and larger than those sensed by Z. The general form is for DDV to be positive in rain where more oblate particles are faster falling, negative within the melting layer and small but slightly negative in ice. In rain, DDV can be used to derive values of m in a gamma drop size distribution, which are always positive, ranging from around 2 to around 8 with 5 being a typical mean. A change in m value from 0 to 10 corresponds to a decrease in rainfall rate of about 30 percent if Z and Z_{DR} are used to calculate the rainfall rate. DDV may also improve our understanding of ice aggregation.

Acknowledgements. We thank the RCRU at RAL for use of the Chilbolton radar, and DRW acknowledges a Gassiot scholarship from the U.K. Met. Office. The work was supported by NERC grants GR3/8523 and GST/02/718.

4 REFERENCES

Beard, K.V., and Chuang, C., 1987: A new model for the equilibrium shape of raindrops. *J. Atmos. Sci.*, **44**, 1509-1524

Goddard, J.W.F., and Cherry, S.M. 1984a: The ability of dual-polarization radar (copolar linear) to predict rainfall rate and microwave attenuation. *Radio Science*, **19**, 201-208

Goddard, J.W.F., and Cherry, S.M. 1984b: Quantitative precipitation measurements with dual linear polarisation radar. Preprints 22nd Conf. on Radar Meteorology held in Zurich, Switzerland.

Gunn, R., and Kinzer, G.D., 1949: The terminal velocity of fall for water drops in stagnant air. *J. Meteor.*, **15**, 452-461

Metcalf, J.I., 1986: Interpretation of the autocovariance and cross-covariance from a polarization diversity radar. *J. Atmos. Sci.*, **21**, 2479-2498

Russchenberg, H.W.J., 1993: Doppler polarimetric radar measurements of the gamma drop size distribution of rain. *J. Appl. Meteor.*, **32**, 1815-1825

Ulbrich, C.W., and Atlas, D., 1984: Assessment of the contribution of differential polarization to improved rainfall measurements. *Radio Science*, **19**, 49-57

11 A.4

THE EFFECT OF ICE CRYSTAL DENSITY ASSUMPTION IN INFERRING REFLECTIVITY VS ICE CONTENT RELATIONSHIP.

Marielle E J Gosset *
ORSTOM, Laboratoire d'études des Transferts en Hydrologie et dans l'Environnement
Grenoble, FRANCE

Anthony J Illingworth, Philip R A Brown and John W G Thomason
JCMM, Dept. of Meteorology, University of Reading, U.K.

1. INTRODUCTION

There is currently a renewed interest in the use of millimetric radar for the monitoring of ice clouds because of the importance of such clouds in the Earth radiation budget. The ability to provide range resolved profiles of cloud structure, together with high sensitivity and good spatial resolution are among factors which make millimetric radar attractive. In addition, the usual drawback of attenuation at short wavelengths is shown to be much reduced in ice clouds.

On the other hand, the high variability of ice crystal habits in natural clouds makes it difficult to relate the radar reflectivity, Z, to the cloud ice water content, IWC, with sufficient accuracy.

Sassen (1987) has proposed a relationship between Z and IWC, valid for cirrus and the upper part of stratiform clouds:

$$IWC = a Z^b, \qquad (1)$$

with a = 0.118 and b = 0.7, where IWC is in $g.cm^{-3}$ and Z is referred to water drops of the same size, at cm wavelengths (cf eq. 3 below). The coefficients were derived from observed ice particle spectra, assuming Rayleigh scattering and using a value of the dielectric factor appropriate for density of 0.92 g cm^{-3}. However, most of atmospheric ice crystals are made of a mixture of ice and air, and many observations have shown that their density tend to decrease when their size increase.

In this paper we examine the effect this density variation has on IWC retrievals at millimetric wavelengths. In situ observations are used to analyse the spread in the coefficients a and b (eq 1) for realistic values of size and density, and accounting for non-Rayleigh scattering.
Calculations are carried out for 3 wavelengths within the millimetric band - namely 35, 78 and 94 Ghz.

2. RADAR PROPERTIES OF ICE PARTICLES.

2.1 Observations of ice particle density

Brown and Francis (1995) have compared the ice water content derived from particle spectra with that obtained from a total ice water content device and show that the cirrus particle density is not constant, but the data were consistent with a density which decreased with particle size:

$$\rho = 0.07\, D^{-1.1} \qquad (2)$$

where D is in mm. This implies that the density of particles is the one of pure ice (ρ_i=0.92 g cm^{-3}) up to about 100µm size, but falls to only 0.07 for 1mm sized particles. (2) is used to describe "low density" particles.

2.2 Dielectric constant and radar reflectivity

In this section we consider ice particles modelled as spheres made of a mixture of ice and air.
In this case, the reflectivity of a crystal of diameter D, is a function of 2 variables only: $x=\pi D/\lambda$, where λ is the wavelength, and ε the dielectric constant of the mixture.
In the lower part of the size spectrum ($x \leq .1$) the expression of reflectivity as a function of D and ε is well approximated by the simple Rayleigh formula:

$$Z = \sum (|K^2| D^6) / 0.93 \qquad (3)$$

where $\sum$ is applied over the full range of diameters, $K = (\varepsilon-1)/(\varepsilon+2)$ and the factor 0.93 is used so that Z is referred to the reflectivity of water drops at λ=10 cm

* M Gosset, LTHE/ORSTOM, BP 53, 38041 Grenoble cedex 9, FRANCE. (Marielle.Gosset@hyrog.fr)

The dielectric constant of a mixture of ice + air can be calculated knowing:

- the dielectric constant of ice ε
- the ratio of the density of the mixture to the density of pure ice ρ_i.

We tried 3 models proposed in the literature:

1. The simple Debye formula, in which, the ratio $|K|/\rho$ is held constant and equal to its value for pure ice, whatever the density of the mixture.
2. The Maxell-Garnett (1904) model in which the particles comprise inclusions of air in a matrix of ice
3. 2, with inclusions of ice in air.

For the dielectric constant of ice ε_i input in the three models, we compared the formulae given by Ray (1972) used by most authors, and the updated version proposed Liebe et al (1989) on the basis of new laboratory measurements. The two show very little difference as far as the real part of ε, is concerned, and give similar results for reflectivity, but lead to very different values of attenuation.

In table 1 below, we show some results for the three models in terms of $|K^2|$, at 0°, at 94 Ghz, and 2 values of density. The values for 35 and 78 GHz are similar.

Table 1:

density ρ	0.92 g cm^{-3}	0.092
K^2 model 1	0.174	0.174e-2
2	for all	0.262e-2
3	models	0.203e-2

In the following calculations we have used model two.

(3) is applicable for Rayleigh scattering, but for larger particles and higher frequencies the complete Mie expression must be used.

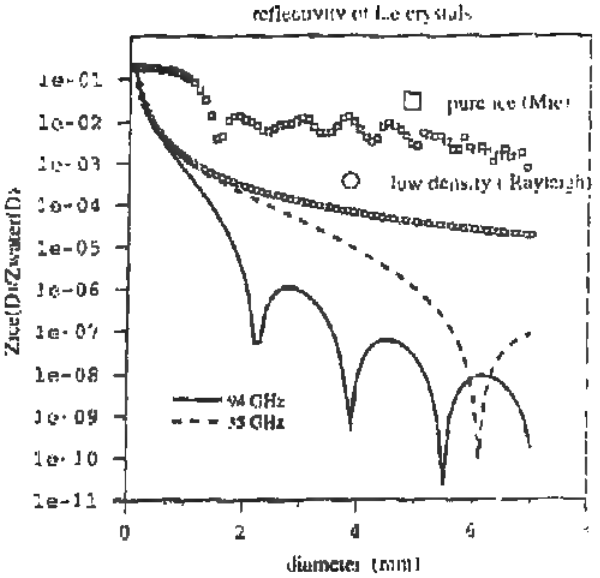

Figure 1 : The reflectivity of single particles as a function of diameter.
Circles show the frequency independent Rayleigh scattering for particles with density dependence given by (2). Mie scattering gives the solid (94GHz) and dotted (35GHz) lines. Squares show Mie scattering for pure ice at 94GHz.

3. RESULTS.

3.1 Reflectivity versus IWC

Figure 2 illustrates the application of the calculations above in terms of Z(IWC) at 94GHz. assuming an exponential ice particle size distribution of the form,

$N(D)=No \exp(-3.67\, D/Dmed)$ (4)

For the two values of Dmed, the spread in Z at fixed IWC is reduced by 20 dB when (2) is used instead of pure ice, and non-Rayleigh scattering accounted for.

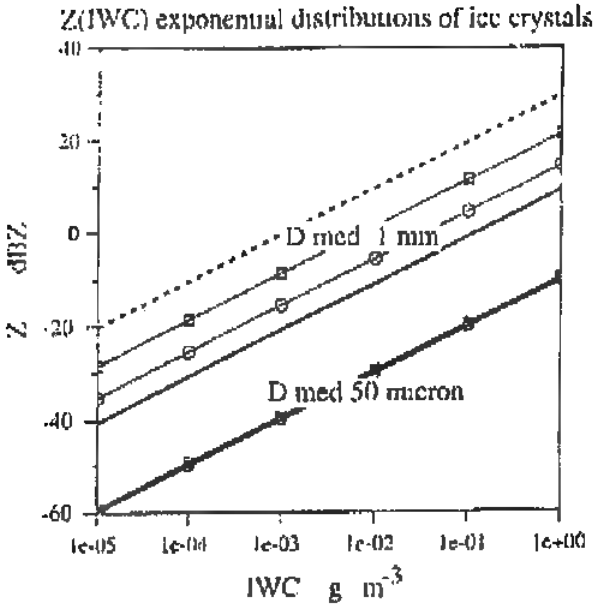

Figure 2: Z versus IWC for Dmed of 50μm or 1 mm. For Dmed = 1mm, the four curves show: (i) pure ice and Rayleigh scattering (dashed), (ii) pure ice and Mie scattering (squares), (iii) low density and Rayleigh scattering (circles), (iv) low density and Mie scattering (solid line).

3.2 effect of density on attenuation

For spherical particles of diameter 1mm the attenuation coefficients per unit IWC at 35, 78 and 94GHz are 0.07, 1.7, 3.4 dB $km^{-1}/g\ m^{-3}$, respectively. For the low density assumption (2) these values are reduced to 0.01, 0.1, 0.2 dB $km^{-1}/g\ m^{-3}$, respectively. For the cirrus data set used by Brown and Francis (1995), we found that the coefficient of attenuation at 94 Ghz, in any part of the cloud, should be less then 0.1 dB km-1. If all particles were assumed to be pure ice then values higher than 10 dB km-1 would be predicted

3.3 Polarisation consideration

Calculations of co-polar returns at horizontal and vertical polarisation from oblate spheroids with various axial ratios, show that no significant polarisation difference is to be expected from the low density particles in cirrus or the upper parts of stratiform clouds. The differential reflectivity, ZDR, should be close to zero and the linear depolarisation ratio, LDR, falls below the detectability threshold of current radars.

4. CONCLUSION

The high variability of ice particle characteristics and sizes in natural clouds leads to considerable scatter in the values of Z for a given IWC, but incorporating realistic density variations together with Mie scattering by the larger particles at millimetric wavelengths reduces this scatter by two orders of magnitude. The lower densities also lead to negligible attenuation by the ice at 94GHz and a reduced sensitivity to polarisation effects.

Dual parameter techniques have recently been explored for deriving ice particle size, either by the use of two radar wavelengths (Matrosov, 1993), combined lidar and radar (Intrieri et al, 1993) or combined radiometer and radar (Matrosov et al, 1992). These methods all assume ice densities of 0.92 g cm-3 and may need reappraisal.

5. ACKNOWLEDGMENTS

This research was carried out as part of the UK Spaceborne Cloud Radar Feasibility Study and with support from NERC grant GR3/8765. The JCMM is supported by the UK Met Office and the University of Reading.

6.REFERENCES

Brown P R A and P N Francis, 1995: Improved measurement of the ice water content in cirrus using a total water evaporator. J Atmos and Ocean Tech, 10, 579-590.

Intrieri J M, Stephens G L, Eberhard W L and Uttal T. ,1993: A method for determining cirrus cloud particle sizes using lidar and radar backscatter technique. J Appl Met, 32, 1074-1082.

Liebe H J, Manabe T and G A Hufford , 1989: Millimeter-wave attenuation and delay rate due to clouds/fog conditions. IEEE AP, 37, 1617-1623.

Matrosov S Y, 1993: Possibilities of cirrus particle sizing from dual-frequency radar measurements. J Geophys Res, 98, 20, 675-683.

Matrosov S.Y., T Uttal, J B Snider, and R A Kropfli, 1992: Estimation of ice cloud parameters from ground-based infrared radiometer and radar measurements. J Geophys Res, 97, 11, 567-574

Sassen, K, 1987: Ice cloud content from radar reflectivity. J Clim and Appl Meteorol, 26, 1050-1053.

CURRENT JCMM INTERNAL REPORTS

This series of JCMM Internal Reports, initiated in 1993, contains unpublished reports and also versions of articles submitted for publication. The complete set of Internal Reports is available from the National Meteorology Library on loan, if required.

1. **Research Strategy and Programme.**
   K A Browning et al
   January 1993

2. **The GEWEX Cloud System Study (GCSS).**
   GEWEX Cloud System Science Team
   January 1993

3. **Evolution of a mesoscale upper tropospheric vorticity maximum and comma cloud from a cloud-free two-dimensional potential vorticity anomaly.**
   K A Browning
   January 1993

4. **The Global Energy and Water Cycle**
   K A Browning
   July 1993

5. **Structure of a midlatitude cyclone before occlusion.**
   K A Browning and N Roberts
   July 1993

6. **Developments in Systems and Tools for Weather Forecasting.**
   K A Browning and G Szejwach
   July 1993

7. **Diagnostic study of a narrow cold frontal rainband and severe winds associated with a stratospheric intrusion.**
   K A Browning and R Reynolds
   August 1993

8. **Survey of perceived priority issues in the parametrizations of cloud-related processes in GCMs.**
   K A Browning
   September 1993

9. **The Effect of Rain on Longwave Radiation.**
   I Dharssi
   September 1993

10. **Cloud Microphysical Processes - A Description of the Parametrization used in the Large Eddy Model.**
H Swann
July 1994

11. **An Appreciation of the Meteorological Research of Ernst Kleinschmidt.**
A J Thorpe
May 1992

12. **Potential Vorticity of Flow Along the Alps.**
A J Thorpe, H Volkert and Dietrich Heimann
August 1992

13. **The Representation of Fronts.**
A J Thorpe
January 1993

14. **A Parametrization Scheme for Symmetric Instability: Tests for an Idealised Flow.**
C S Chan and A J Thorpe
February 1993

15. **The Fronts 92 Experiment: a Quicklook Atlas.**
Edited by T D Hewson
November 1993

16. **Frontal wave stability during moist deformation frontogenesis. Part 1. Linear wave dynamics**
C H Bishop and A J Thorpe
May 1993

17. **Frontal wave stability during moist deformation frontogenesis. Part 2. The suppression of non-linear wave development.**
C H Bishop and A J Thorpe
May 1993

18. **Gravity waves in sheared ducts.**
S Monserrat and A J Thorpe
October 1993

19. **Potential Vorticity and the Electrostatics Analogy: Quasi-Geostrophic Theory.**
C Bishop and A J Thorpe
November 1993

20. **Recent Advances in the Measurement of Precipitation by Radar.**
A J Illingworth
April 1993

21. **Micro-Physique et Givrage. Cloud Microphysics and Aircraft Icing.**
A J Illingworth
May 1993

22. **Differential Phase Measurements of Precipitation.**
M Blackman and A J Illingworth
May 1993

23. **Estimation of Effective Radius of Cloud Particles from the Radar Reflectivity.**
N I Fox and A J Illingworth
May 1993

24. **A Simple Method of Dopplerising a Pulsed Magnetron Radar.**
L Hua, A J Illingworth and J Eastment
November 1993

25. **Radiation and Polar Lows.**
George C Craig
February 1994

26. **Collected preprints submitted to International Symposium on the Life Cycles of Extratropical Cyclones; Bergen, Norway, 27 June - 1 July 1994**
April 1994

27. **Convective Frontogenesis**
Douglas J Parker and Alan J Thorpe
April 1994

28. **Improved Measurement Of The Ice Water Content In Cirrus Using A Total Water Evaporator**
Philip R A Brown and Peter N Francis
April 1994

29. **Mesoscale Effects of a Dry Intrusion within a Vigorous Cyclone**
K A Browning and B W Golding
April 1994

30. **GEWEX Cloud System Study, Science Plan**
May 1994

31. **Parametrization of Momentum Transport by Convectively Generated Gravity Waves**
R Kershaw
February 1995

32. **Mesoscale Modelling Newsletter, No. 5**
May 1994

33. **Observations of the mesoscale sub-structure in the cold air of a developing frontal cyclone**
K A Browning, S A Clough, C S A Davitt, N M Roberts and T D Hewson
May 1994

34. **Longwave Radiative Forcing of a Simulated Tropical Squall Line**
Imtiaz Dharssi
July 1994

35. **On the nature of the convective circulations at a kata-cold front**
K A Browning
September 1994

36. **Collected preprints of papers submitted to the COST-75 International Seminar on Advanced Weather Radar Systems, Brussels, 20-23 September 1994**
November 1994

37. **Use of satellite imagery to diagnose events leading to frontal thunderstorms: Parts I and II of a case study**
K A Browning and N M Roberts
November 1994

38. **The role of spaceborne millimetre-wave radar in the global monitoring of ice cloud**
P R A Brown, A J Illingworth, A J Heymsfield, G M McFarquhar, K A Browning and M Gosset
December 1994

39. **Potential Vorticity Inversion**
Michal Ziemianski
October 1994

40. **Theory of mature tropical cyclones; A comparison between Kleinschmidt (1951) and Emanual (1986)**
Suzanne L Gray
December 1994

41. **Dispersion and removal of pollutants during the passage of an atmospheric frontal system**
N R Gimson
December 1994

42. **The role of snow sublimation in frontogenesis**
D J Parker and A J Thorpe
December 1994

43. **Potential vorticity and the electrostatics Analogy: Ertel-Rossby formulation**
A J Thorpe and C H Bishop
December 1994

44. **Mesoscale aspects of extratropical cyclones: an observational perspective**
K A Browning
January 1995

45. **A Polar Low Outbreak: Evolution and Mesoscale Structures**
T D Hewson, G C Craig and C Claud
February 1995

46. **Generation of near-surface gusts by deep convection**
K Nakamura and R Kershaw
April 1995

47. **Attribution concepts applied to the omega equation**
S A Clough, C S A Davitt and A J Thorpe
June 1995

48 **Parametrization of mixed-phase cloud and precipitation**
Susan P Ballard and M Gerard Hutchinson
June 1995

49 **Short-range forecasting of stratocumulus: Initialization V Prediction**
Susan P Ballard, Simon D Jackson and B Macpherson
June 1995

50 **Contributions of the JCMM/Dept of Meteorology Radar Group to the 27th AMS Radar Meteorology Conference, Vail October 1995**
June 1995

Met Office Joint Centre for Mesoscale Meteorology Department of Meteorology
University of Reading PO Box 243 Reading RG6 6BB United Kingdom
Tel: +44 (0)118 931 8425 Fax: +44 (0)118 931 8791
www.metoffice.com